國立交通大學

電信工程學系

碩士論文

設計微小化與寬拒帶之超寬頻濾波器

A Simple Design Methodology for Compact Ultra-Wideband Filter with Wide-Stopband

研 究 生： 翁昭竹

指導教授 ： 周復芳 博士

中華民國九十八年三月

設計微小化與寬拒帶之超寬頻濾波器

A Simple Design Methodology for Compact Ultra-Wideband Filter with Wide-Stopband

研 究 生 ： 翁昭竹 　　Student ： Zhao-Zhu Wong

指導教授 ： 周復芳 博士 　　Advisor : Dr. Christina F. Jou

國立交通大學

電信工程學系碩士班

碩士論文

A Thesis
Submitted to Department of Communication Engineering
College of Electrical and Computer Engineering
National Chiao Tung University
In Partial Fulfillment of the Requirements
for the Degree of
Master of Science
in Communication Engineering

March 2009

Hsinchu, Taiwan, Republic of China

中華民國九十八年三月

設計微小化與寬拒帶之超寬頻濾波器

研究生 : 翁昭竹　　　　　　　　　　指導教授 : 周復芳 博士

國立交通大學電信工程學系碩士班

中文摘要

本篇論文將介紹一個簡易的方法來設計一個超寬頻的集總(lumped)濾波器。本篇所提出的方法，是利用傳輸極點(transmission poles)來設計頻帶內的特性,以及利用傳輸零點(transmission zeros)來改善拒帶的響應。 最後利用史密斯圖的匹配方法求出電路中被動元件的值。另一方面，因為此架構只由八個被動元件所組成而且同時利用上層與下層金屬來設計電路架構，所以具有微小的電路面積。而最後量測結果顯示所設計的濾波器具有以下特性，3dB 頻寬為 128% (2.8GHz ~ 11.4GHz)，頻帶內返回損耗最小值為 0.3dB，在 12.4 GHz 到 23.7 GHz 的頻帶內，其拒帶之嵌入損耗皆大於 20dB，具有非常微小的電路尺寸 0.23 λ × 0.31 λ，其中 λ 是在微帶線結構中中心頻率為 7.1 GHz 的導波波長。此外由量測資料我們也可以求的其濾波器其群延遲在整個頻帶內變動範圍為 0.32 ns 到 0.46 ns。

A Simple Design Methodology for Compact Ultra-Wideband Filter with Wide-Stopband

Student : Zhao-Zhu Wong Advisor : Dr. Christina F. Jou

Department of Communication Engineering

College of Electrical and Computer Engineering

National Chiao Tung University

Abstract

This paper proposes a simple methodology for designing a wideband compact LC-filter. According to the proposed methodology, given the transmission zeros which can construct the in-band characteristic and the transmission zeros which can improve stopband rejection, the filter's component values can be obtained graphically on the Smith chart. Additionally, because the filter only consists of eight lumped components, which is implemented at both top and bottom layer, it has compact size. The measured results shows that the filter prototype has a measured 3-dB fractional bandwidth of 128% from 2.8 GHz to 11.4 GHz, minimum insertion loss of 0.3 dB within the pass-band, superior 20 dB stop-band rejection from 12.4 GHz to 23.7 GHz, and very compact circuit size of 0.23 λ × 0.31 λ, where λ is the guided wavelength of the microstrip structure at the center frequency f_0 = 7.1 GHz. Moreover, from the measured S-parameters, we obtain that the developed filter with the feeding lines exhibits flat group-delay response ranging from 0.32 ns to 0.46 ns over the whole passband.

誌謝

在這充實的研究生生涯裡，首先要先感謝周復芳老師的指導，讓我不只學習到課業上的知識，也學習到一些研究應該有的態度。同時也感謝胡樹一老師以及張志揚老師對於此論文的指導與意見，讓此研究能更加整體化以及完善。也謝謝陳伯寧主任在待人處事上給了我很多寶貴的意見。

在學習前期，謝謝 pu、力尹、鐵人、明達、青峰和阿良學長的指導，讓剛成為研究生的我倍感溫馨，更加謝謝龍哥以及血牛陪同我度過了一年半的研究生生涯，謝謝你們的關心以及鼓勵，同時也要謝謝 37，能在我最難熬的時候，讓我有一個說話的空間，另外也要謝謝在科專計畫中一直鼓勵我以及教導我的許立翰學長和資鑫學長，對於妳們的關心，我感到非常的窩心。

在學習後期，謝謝奕霖，玠瑝，硬漢，安東尼，班森，沛遠，智元，小老鼠，因為有你們，讓我更加的融入這個大環境裡。也謝謝智鵬，宜星，俊緯學長的指導，此外還有碩一的學弟們與我分享一些生活上的點滴。在這裡，大家一起認真做研究，一起開心的打球，對我來說是一段很美好的回憶，而最感謝的是指導我的匯儀學長，讓當時居無定所的我有了落地生根的地方，沒有他，就不會有現在的我，謝謝學長花了很多時間指導我與解答我研究上的疑問，能有這樣一位學長帶著我做研究，讓我由衷的感謝。

最後要謝謝我的家人，在研究生生涯裡，儘管我有一些無理的要求，但仍一直在背後支持著我，鼓勵著我，與我分享開心與不開心的事物，我愛妳們。

翁昭竹

于 新竹交大

2009 春

CONTENTS

List of Tables

List of Figures

Chapter 1

INTRODUCTION

1.1 Background and motivation

Wide-band bandpass filters (BPF's) have been a critical component for both scientific community and the communication industry, such as radio astronomy receivers and ultra-wideband (UWB) technologies. A superior wideband filter should have not only low insertion loss and flat group delay over its pass-band, but also have good selectivity at both pass-band edges. Also, compact size is preferred. In addition, to reduce the interference from existing communication systems, good stop-band rejection is also required.

Due to the demand of UWB filter application, different kinds of filter's structure had been introduced. The following are some various techniques to design wideband filter, and we will discuss its advantage and disadvantage.

First of all, filters using microstrip ring have been studied in [1], which have good insertion loss and sharp rejections, but suffer from poor out-of-band performance due to the strong spurious response.

Example in [1]

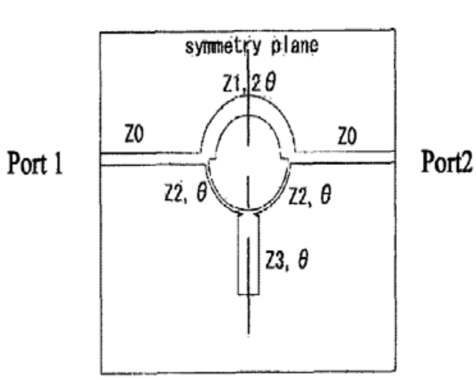

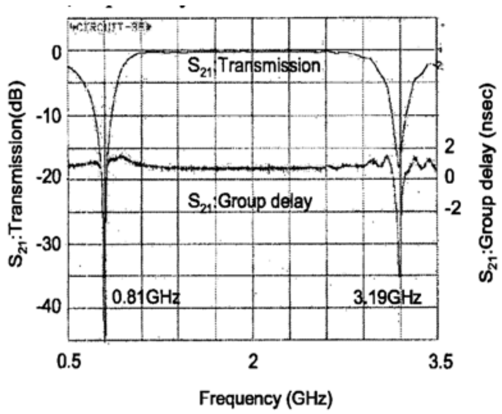

Secondly, the filters using parallel-coupled lines with defected ground were employed to give a tight coupling for wideband application [2] and [3]. However, owing to the stringent requirement of large fractional bandwidth, very small gap size is demanded to enhance the coupling, which is not easy to be fabricated. One way to relieve the restriction on gap size is to add a third line in the parallel coupled-line filter, unfortunately, the necessary gap size is still too narrow to be fabricated [4].

Example in [2] and [3]

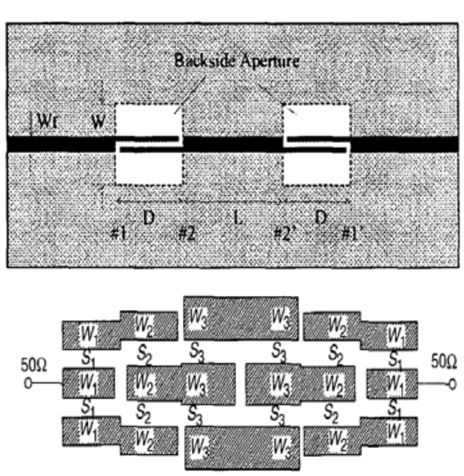

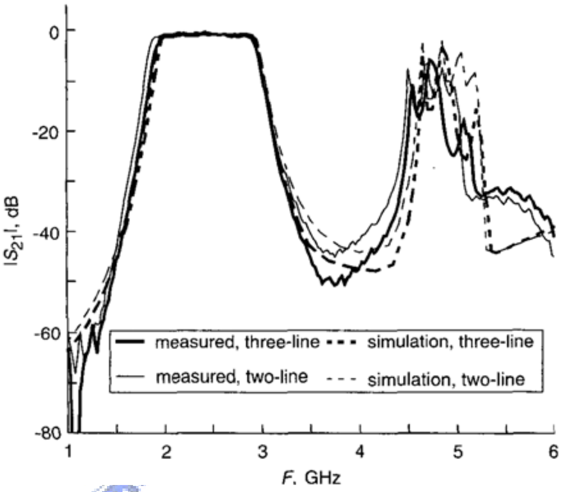

Last, there are similar awkward situations in filters adopting multimode resonators in [5]-[7]. These filters shown the low insertion loss and flat group delay over the pass band, but may lead to poor spurious response and small gaps.

Example in [5]

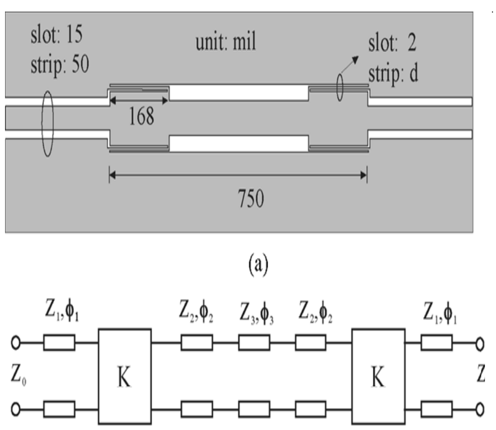

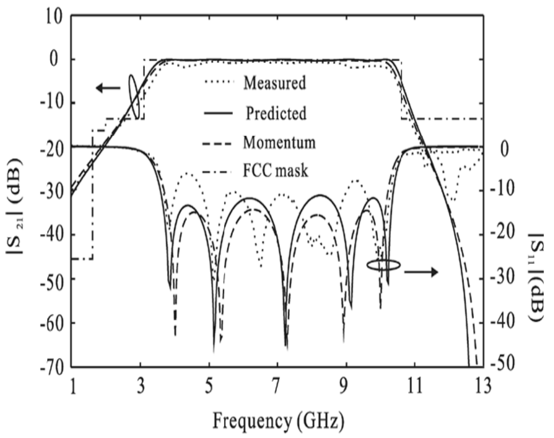

To suppress spurious response, cascading low-pass and high-pass filters have been reported in [8] and/or cascading band-stop and band-pass filters in [9]. These wideband filters have excellent out-of-band responses, but they occupy large circuit size and large insertion loss.

Example in [8]

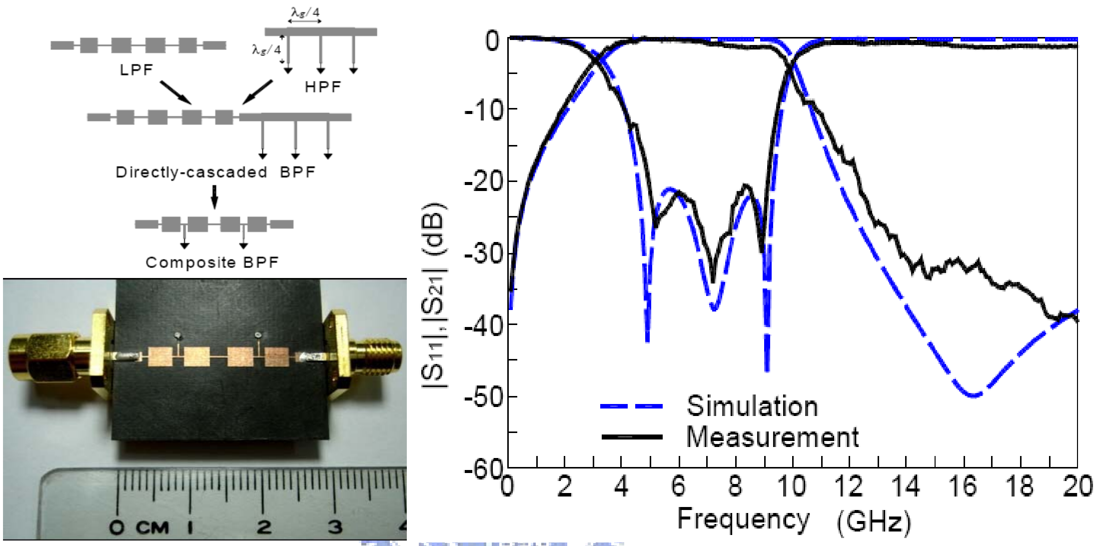

Example in [9]

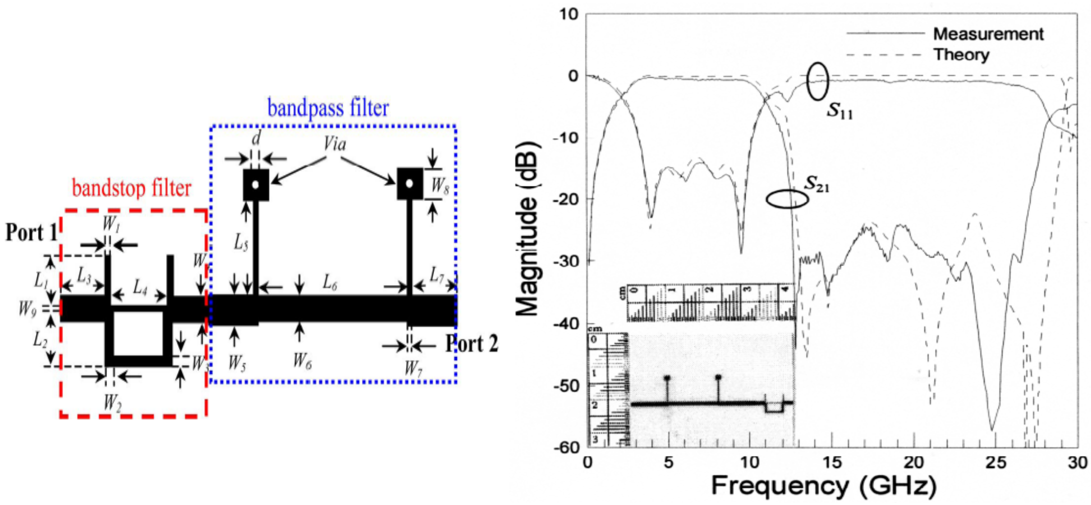

Besides, electromagnetic bandgap structures are also applied to improve out-of-band rejection in [10] and [11], but it still occupies too large circuit size.

Example in [10]

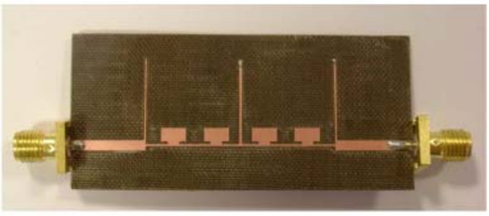

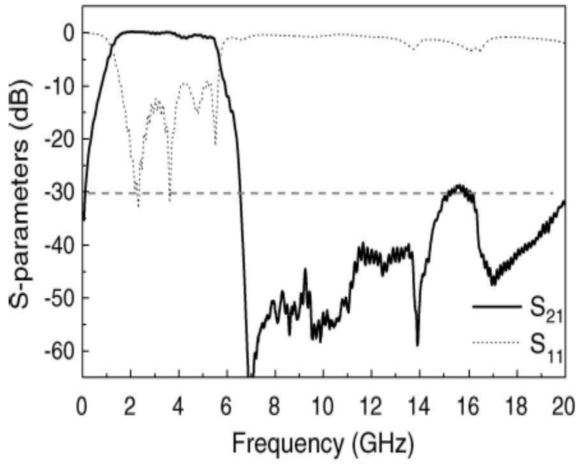

Another way to design wideband filters with improved upper stop-band performance is using quasi-lumped elements [12], however, the circuit size and insertion loss can still be further minimized.

Example in [12]

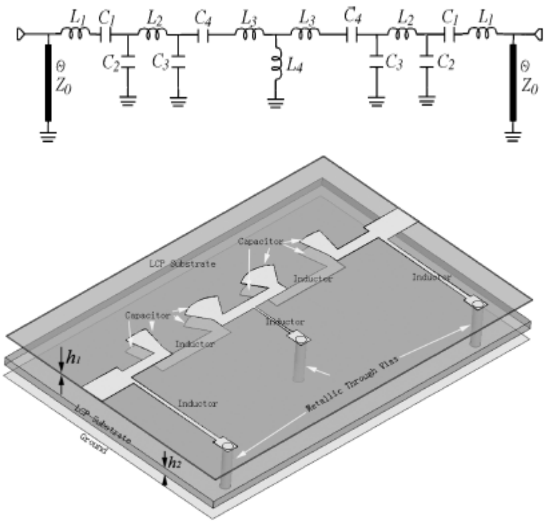

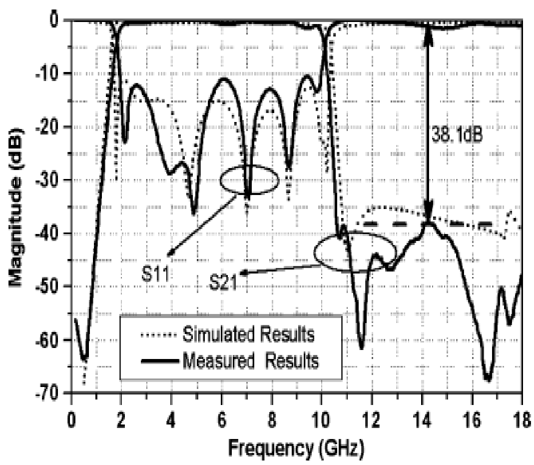

According to the discussion above in [8] ~ [12], we find that they are useful technique to suppress the harmonic response, but they also occupy big circuit size. Thus, in this paper we want to propose a new method to construct compact ultra-wideband filter and reduce the circuit size in the same time. In addition, in many published literatures, there are confusions on how an awful lot of tuning is still required even with the much-revered mathematical underpinnings, which also prompts the research of this paper.

1.2 Thesis organization

In chapter 2, by treating the wideband LC-filter as a matching network [13], the mechanism of the proposed band-pass filter can be easily understood graphically on the Smith chart. Besides, to further improve its stop-band rejection, two transmission zeros are then introduced, the component values of the LC filter can be obtained graphically through the Smith chart, and the relevant equations, which are functions of transmission zeros and poles, are also derived.

In chapter 3, the feasibility of the filter theorem is then supported by the agreements between the simulated results and its calculated counterparts from the developed formulas. A 3 – 10 GHz wideband filters fabricated in Rogers RO4003C (with $\varepsilon_r = 3.5$, $\tan\delta = 0.0027$, and thickness h = 0.508 mm) is demonstrated.

In chapter 4, we will conclude the characteristic of the proposed filter and compare with other type UWB filters.

Chapter 2

A SIMPLE DESIGN METHODLOGY FOR COMPACT ULTRA-WIDEBAND FILTER WITH WIDE-STOPBAND

2.1 Introduction

It's well-known that wide-band bandpass filters (BPF's) have been a critical component for both scientific community and the communication industry. In chapter 1, we have listed different types of wideband bandpass filter and discuss the characteristic of each one. Then, in order to suppress out-of-band harmonic and reduce the circuit size in the same time, the proposed filter has shown in Fig.1.

In Fig. 1, the proposed LC filter only consists of five inductors and three capacitors, it has compact size. Besides, to avoid the mathematical entanglement, we resort to the Smith chart to reveal how simply by the three resonators this wideband LC-filter can achieve its superior wideband characteristic.

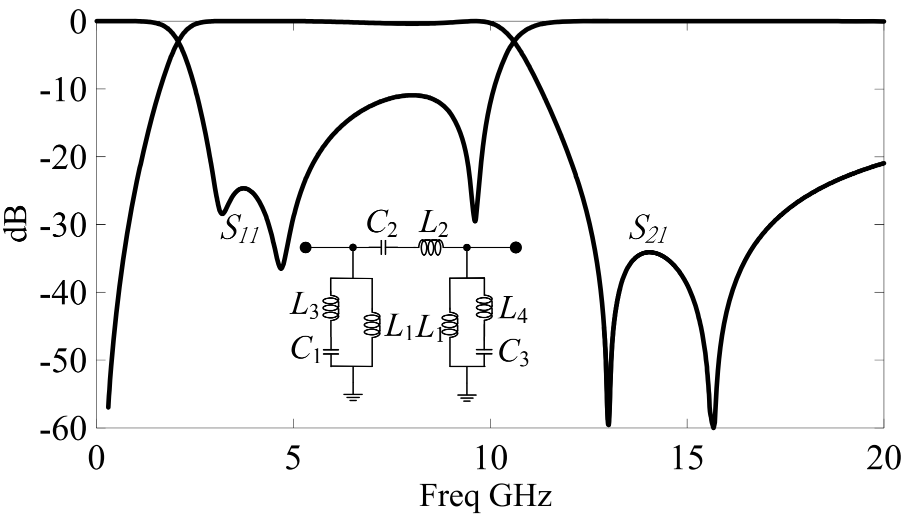

Fig. 1. The circuit layout and the simulated *S*-parameters of the proposed wideband filter.

2.2 Matching criterion for a π-network

2.2.1 Matching mechanism of a π-network

As shown in Fig. 1, the proposed LC filter, which is a π-network, can achieve wideband characteristic, thus we will focus on what a π-network's characteristic is. In Fig. 2(a), a π-network is shown, and the motion of impedance transformation on the Smith chart is shown in Fig. 2(b).

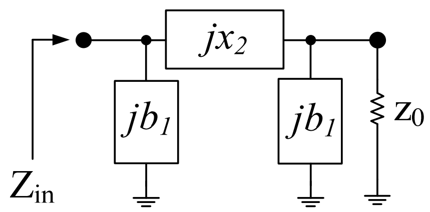

(a)

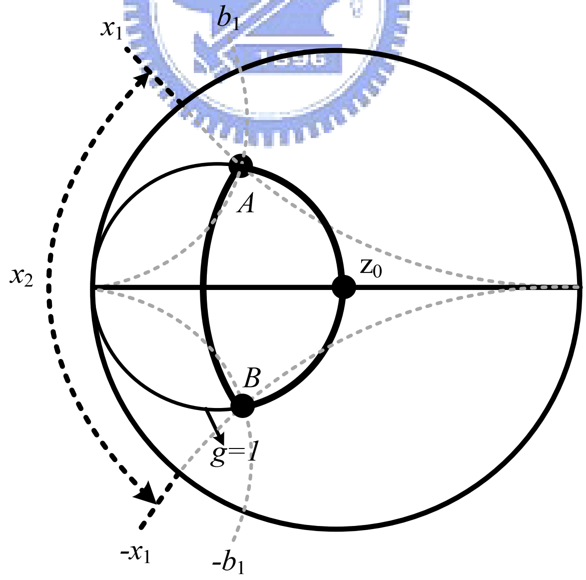

(b)

Fig. 2 (a). π-network, where b_1 is the normalized susceptance, x_2 is the normalized reactance.(b) The impedance transformation of the circuit in the fig. 2(a) where Z_0 is the ubiquitous microwave 50-ohm

In Fig. 2(b), we know that for an arbitrary value of susceptance b_1 will have its corresponding value of reactance x_2 to transform the impedance back to 50 ohm. In order to find out the relationship of b_1 and x_2, we have to solve the value of x_1 first.

On Y-Smith-Chart, the constant g circle can be expressed

$$(u+\frac{g}{1+g})^2+(v^2)=(\frac{1}{1+g})^2 \tag{1}$$

On the other hand, the constant b_1 circle can be expressed

$$(u-1)^2+(v-\frac{1}{b_1})^2=(\frac{1}{b_1})^2 \tag{2}$$

where u and v are the real part and imagine part of reflection coefficient respectively. For g=1, u and v can be express as follow:

$$u=\frac{-b_1^2}{4+b_1^2} \tag{3}$$

$$v=\frac{-2b}{4+b_1^2} \tag{4}$$

Furthermore, the imagine part of normalized impedance can be expressed in terms of u and v

$$x_1=\frac{2v}{(1-u)^2+v^2} \tag{5}$$

Then combine (3), (4), and (5), we can get

$$x_1=\frac{-b_1}{1+b_1^2} \tag{6}$$

In Fig. 2(b), it is clear that if the impedance transformation backs to 50 ohm, it has to satisfy the follow equation:

$$x_2=(-x_1)-x_1=\frac{2b_1}{1+b_1^2} \tag{7}$$

So far, the matching criterion (7) that can make the π-network match to 50 ohm is derived. On the other hand, we can also use ABCD matrix to solve a π-network in Fig. 2(a) to get the matching criterion (7), which will be described in Appendix.

Up to now we have figured out how the mechanism of matching network of the π-network is and the relationship between b_1 and x_1.Then, we will focus on how to choose the proper value of b_1.

2.2.2 Choose of the value of susceptance b_1

After the discussion above in section2.2.1, now we start to find out the value of susceptance b_1. Initially, in fig. 3(a), we take a low-pass circuit, of which $x_2 = \omega L/Z_0$ and $b_1 = \omega CZ_0$, as an example to verify the feasibility of the derived matching criterion (8)

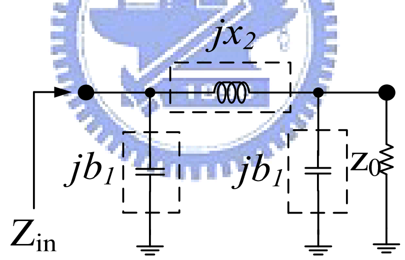

Fig. 3 A low-pass filter

Furthermore, to easily understand the mechanism of the π-network, we treat it as a matching network. Among the solutions that can meet the criterion (7), we just pick out three solutions as examples, $b_1 = 0.6$, 1, and 1.67. As can be seen graphically on the Smith chart, there are three trajectories satisfying (7) can move Z_{in} from 50-ohm termination to a lower resistive impedance, and then to 50-ohm starting point again.

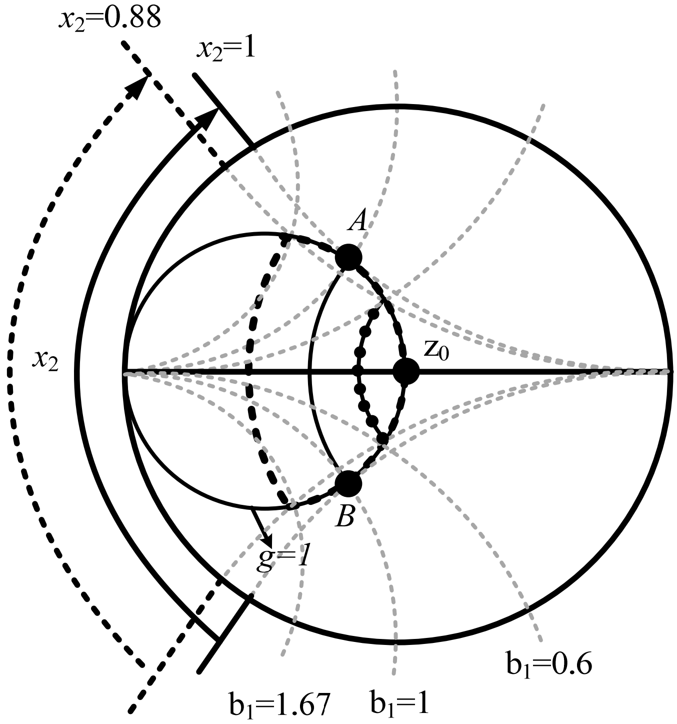

Fig.4 The Z_{in}'s impedance transformation of a low-pass circuit

The solid trajectory is with $b_1 = 1$, $x_2 = 1$, the circled trajectory is with $b_1 = 0.6$, $x_2 = 0.88$, and the dashed trajectory is with $b_1 = 1.66$, $x_2 = 0.88$. When we set ω as 10 GHz, the values of L and C can be obtained in table.1 and its corresponding *S*-parameters are shown in Fig. 5. Notably, although the circled curve has the best matched condition (lowest S_{11}), it has the poorest stop-band roll-off, on the contrary, the dashed curve has the poorest matched condition (lowest S_{11}) while it has the best stop-band roll-off, thus the solid trajectory ($b_1 = x_2 = 1$) is a compromise between the dashed trajectory and circled trajectory and is preferred.

b_1	x_2	L (nH)	C (pF)
0.6	0.88	0.71	0.19
1	1	0.79	0.32
1.67	0.88	0.71	0.53

Table.1 The value of b_1, x_1, L, and C for three solutions for low-pass filter

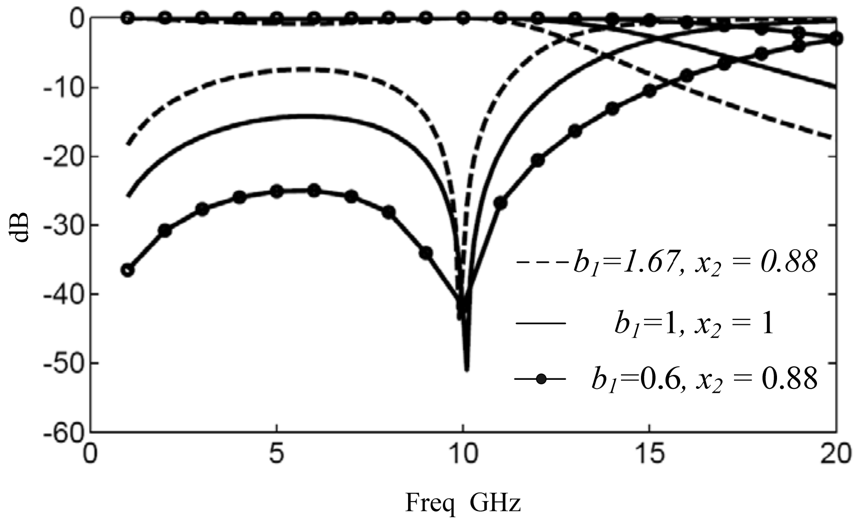

Fig. 5 Three solutions of the low-pass circuit that meet the matching criterion (7).

On the other hand, in the case of high-pass circuit in Fig. 6, it also has the same phenomenon of high-pass filter of which $x_2 = 1/Z_0\omega C$ and $b_1 = Z_0/\omega L$, We set ω as 3 GHz, the values of L and C can be obtained and listed in table.2 and its corresponding *S*-parameters are shown in Fig. 7. As a result, $b_1 = x_2 = -1$ is also suggested in high-pass filter. Thus far, the matching mechanism of the high pass circuit and low pass circuit has been clarified, and the matching criterion (7) is derived. Next, the proposed wideband filter mechanism will be elaborated.

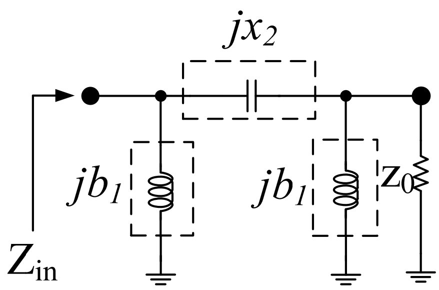

Fig. 6 A high-pass filter

b_1	x_2	L (nH)	C (pF)
-0.6	-0.88	4.42	1.21
-1	-1	2.65	1.06
-1.67	-0.88	1.59	1.21

Table.2 The value of b_1, x_2, L, and C for three solutions for high-pass filter

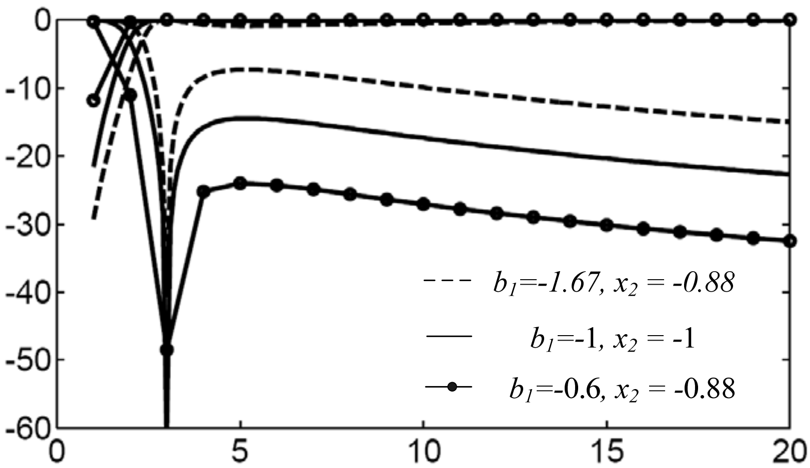

Fig. 7. Three solutions of the high-pass circuit that meet the matching criterion (7).

2.3 Wideband Filter Mechanism

2.3.1 In-band design

After discussing the matching network of a π-network, in this section we will apply the method mentioned in section 2.2.1 and 2.2.2 to explain the proposed filter and give some simple design equations.

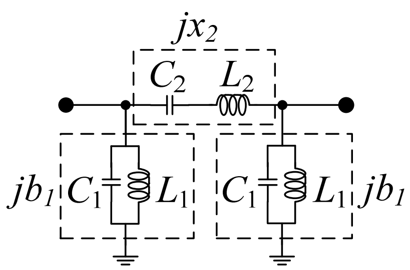

(a)

Fig. 8. (a) The prototypical wideband filter.

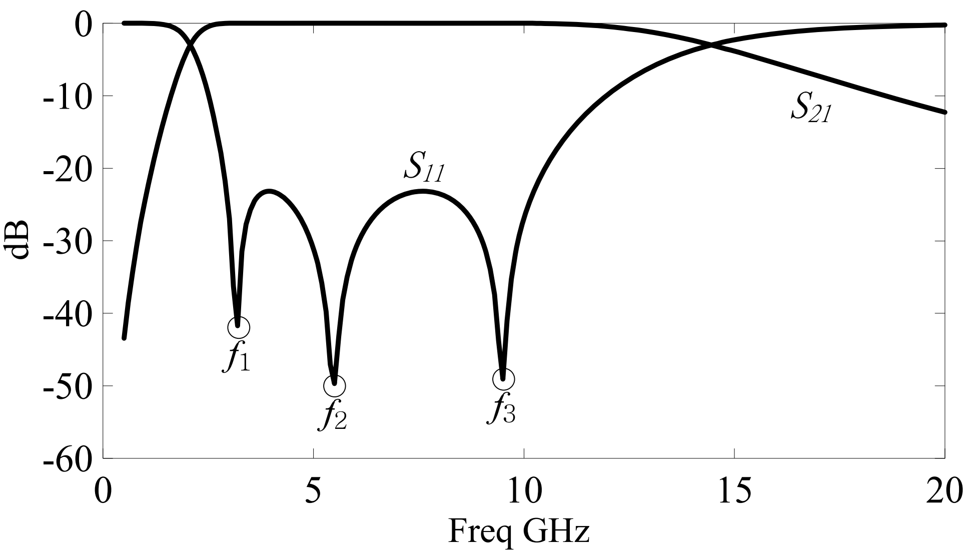

(b)

Fig. 8(b) The corresponding simulated S_{11} and S_{21} with L_1 = 2.65 nH, C_1 = 0.32 pF, L_2 = 1.14 nH, and C_2 = 0.74 pF, where f_1 of 3.1 GHz, f_2 of 5.4 GHz and f_3 of 9.5 GHz are three matched frequencies (transmission poles)

The prototypical wideband filter is shown in Fig. 8(a). In Fig. 8(b), where f_1 of 3.1 GHz (lower in-band), f_2 of 5.4 GHz (mid in-band) and f_3 of 9.5 GHz (higher in-band) are three matched frequencies (or transmission poles). To avoid the mathematical entanglement, we resort to the Smith chart which has been discussed in section 2.2 to reveal how simply by the three resonators this wideband LC-filter can achieve its superior wideband characteristic.

First of all, at lower in-band, the parallel circuit L_1C_1 appears inductive and the series circuit L_2C_2 appears capacitive, so the approximated circuit in Fig. 9 applies, and its corresponding high-pass characteristic with its matched frequency f_1 (= 3 GHz) is shown. And Fig. 10 is the impedance transformation of low-pass filter

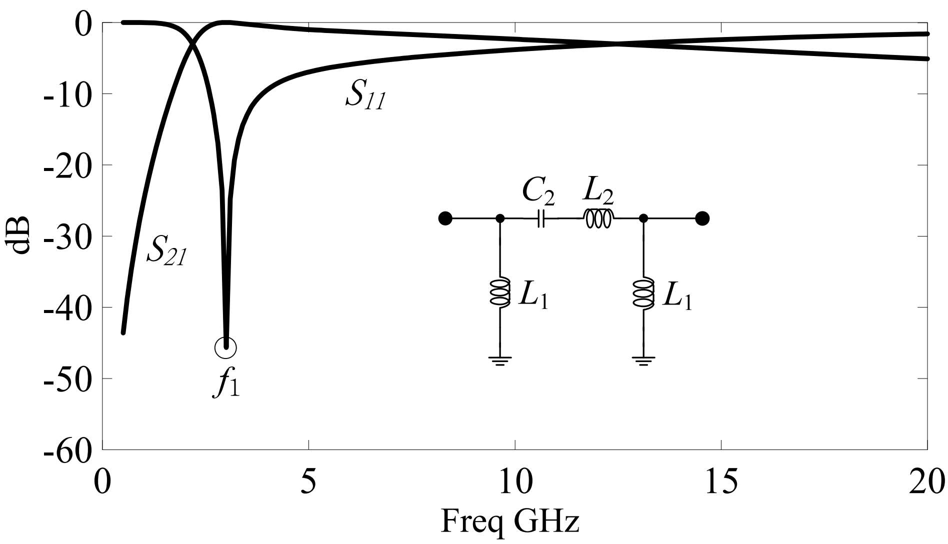

Fig. 9. The simulated S_{11} and S_{21} of the equivalent high-pass circuit with L_1=2.65nH, L_2 = 1.14 nH, and C_2 = 0.74 pF, where f_1 is its matched frequency (transmission pole).

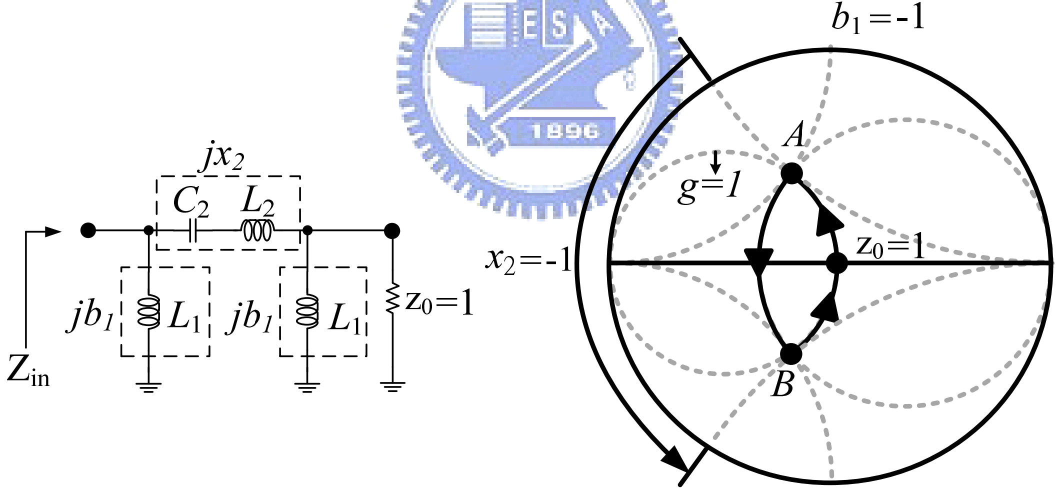

Fig. 10. Z_{in}'s impedance transformation from the normalized termination resistance z_0 = 1 and back up to the z_0 starting point again.

As shown in Fig. 10, owing to the "shunt" inductor L_1, the motion of Z_{in}'s impedance transformation from the normalized termination resistance z_0 = 1 to point A on the Smith chart is along the unit constant-conductance circle (g = 1), and we obtain that the shunt inductor's normalized susceptance equals b_1; then, by series circuit L_2C_2, of which the normalized reactance is x_2, the trajectory of impedance transformation moves from point A to point B; finally, it moves back to the z_0 starting point by the other shunt inductor L_1. As derived in the previous section, $b_1 = x_2 = -1$ is the suggested matching criterion which makes Z_{in} of a high-pass circuit equal 50-ohm. Thus, in Fig. 10, the normalized susceptance b_1 of the inductor L_1 must be -1:

$$jb_1 = \frac{Z_0}{j\omega_1 L_1} = -j1 \tag{8}$$

where ω_1 is the angular frequency corresponding to the f_1, and Z_0 is the ubiquitous microwave 50-ohm, thus L_1 can be determined by the given ω_1 as follow:

$$L_1 = \frac{Z_0}{\omega_1} \tag{9}$$

Then, we can equal the normalized reactance x_2 of L_2C_2 with -1, as follow:

$$jx_2 = \frac{j(\omega_1 L_2 - \frac{1}{\omega_1 C_2})}{Z_0} = -j1 \tag{10}$$

Secondly, at higher in-band, the parallel circuit L_1C_1 appears capacitive and the series circuit L_2C_2 is inductive, so the approximated circuit in Fig. 11 applies, and its corresponding low-pass characteristic with its matched frequency f_3 (= 10 GHz) is also shown.

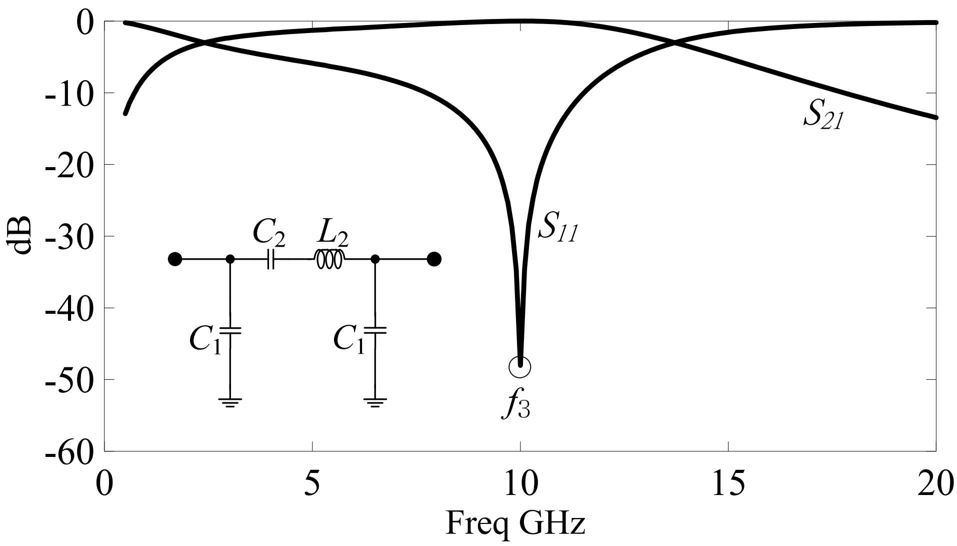

Fig. 11. The simulated S_{11} and S_{21} of the equivalent low-pass circuit with C_1 = 0.32 pF, L_2 = 1.14 nH, and C_2 = 0.74 pF, where f_3 is its matched frequency.

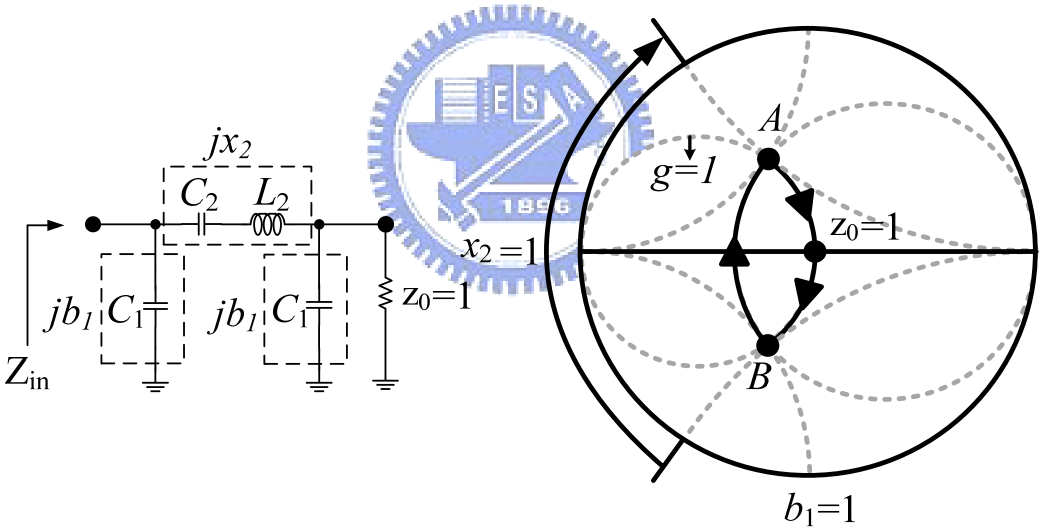

Fig. 12. Z_{in}'s impedance transformation of the equivalent low-pass circuit from the normalized termination resistance z_0 = 1 and back to the z_0 starting point again

As shown in Fig. 12, owing to the "shunt" inductor C_1, the motion of Z_{in}'s impedance transformation from the normalized termination resistance z_0 = 1 to point B on the Smith chart is along the unit constant-conductance circle (g = 1), and we obtain that the shunt capacitor's normalized susceptance equals b_1; then, by series circuit L_2C_2, of which the normalized reactance is x_2, the trajectory of impedance transformation moves from point B to point A; finally, it moves back to the z_0 starting point by the other shunt capacitor C_1. As derived in the previous section, $b_1 = x_2 = 1$ is the suggested matching criterion which makes Z_{in} of a low-pass circuit equal 50-ohm. Thus, in Fig. 12, the normalized susceptance b_1 of the capacitor C_1 must be 1, and can be derived as follow

$$jb_1 = j\omega_3 C_1 Z_0 = j1 \tag{11}$$

where ω_3 is the angular frequency corresponding to the f_3, thus C_1 can be settled by the given ω_3

$$C_1 = \frac{1}{\omega_3 Z_0} \tag{12}$$

Similarly, by series L_2C_2 the trajectory of Z_{in}'s impedance transformation moves from point B to point A, thus we can obtain that the normalized reactance x_2 of L_2C_2 equals 1, as follow:

$$jx_2 = \frac{j(\omega_3 L_2 - \frac{1}{\omega_3 C_2})}{Z_0} = j1 \tag{13}$$

Combine (10) and (13), L_2 and C_2 can be expressed as

$$L_2 = \frac{Z_0}{(\omega_3 - \omega_1)} \tag{14}$$

$$C_2 = \frac{1}{Z_0}\left(\frac{1}{\omega_3} - \frac{1}{\omega_1}\right) \tag{15}$$

Thus far, intuitive exposition of the wideband band-pass filter can now be best understood as follow: at low frequency, it looks like a high-pass circuit and meets $b_1 =$

x_2 = -1 at the lower matched frequency f_1 (transmission pole); at high frequency, it can be regarded as a low-pass circuit and meets $b_1 = x_2 = 1$ at the higher matched frequency f_3 (transmission pole). Therefore, with the given f_1 (ω_1) and f_3 (ω_3), L_1, C_1, L_2, and C_2 can be manipulated by (9), (12), (14), and (15), respectively. Finally, substitute f_1 = 3 GHz, and f_3 = 10 GHz in (9), (12), (14), and (15), L_1 = 2.65 nH, C_1 = 0.32 pF, L_2 = 1.14 nH, C_2 = 0.74 pF can be derived. Its corresponding simulated results, as shown in Fig. 8, exhibiting three matched frequency (transmission zeros) 3.1GHz, 5.4GHz, and 9.5 GHz thereupon confirms the accuracy of the previously derived equations. In addition, with the derived components values, both the resonance frequency of the series circuit L_1C_1 and that of the parallel circuit L_2C_2 are at 5.4 GHz, that is, Z_{in} equals the termination resistance Z_0 (50 ohm) at this resonance frequency, thus, there is a matched frequency ω_2 of 5.4 GHz. In conclusion, we can use transmission zero to design a filter's in-band characteristic.

2.3.2 Stop-band design

In addition to the required in-band response characterized in the previous section, the stop-band rejection is now concerned and can be improved by introducing transmission zeros at the stop-band

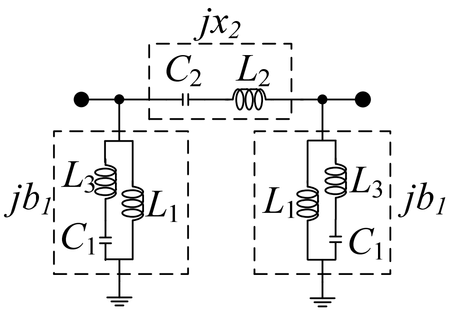

(a)

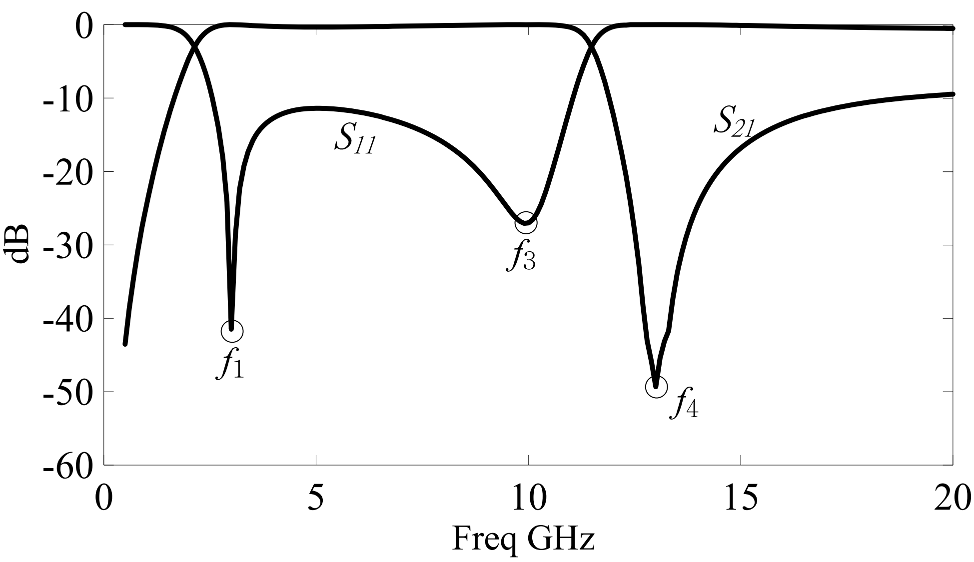

(b)

Fig. 13 (a) The modified prototypical filter (b) The simulated S_{11} and S_{21} of the (a) with L_1 = 2.65 nH, L_2 = 1.14 nH, L_3 = 1.15nH, C_1 = 0.13 pF, and C_2 = 0.74 pF, where f_1 and f_3 are the matched frequencies (transmission poles), f_4 is the transmission zero.

In addition to the required in-band response characterized in the previous section, the stop-band rejection is now concerned and can be improved by introducing transmission zeros at the stop-band. With the short circuit nature of a series circuit, replacing C_1 with the series circuit L_3C_1, as depicted in Fig. 13(a), can construct a transmission zero at f_4, as illustrated in Fig. 13(b). If we adopt the same design methodology described in the previous section: at low frequency, it looks like a high-pass circuit and meets $b_1 = x_2 = -1$ at the lower matched frequency f_1 (transmission pole); at high frequency, it can be regarded as a low-pass circuit and meets $b_1 = x_2 = 1$ at the higher matched frequency f_3 (transmission pole). Thus, the value of L_1 can be determined by (9) (i.e. b_1 = -1 at f_1), L_2C_2 can be determined by ω_1 and ω_3 through (14), and (15) (i.e. x_2 = -1 and 1 at f_1 and f_3, respectively); in addition, the normalized susceptance b_1 of the series circuit L_3C_1 equals 1 at the higher matched frequency f_3, as follow:

$$jb_1 = \left(\frac{j\omega_3 L_3}{Z_0} + \frac{1}{jZ_0\omega_3 C_1} \right)^{-1} = j1 \qquad (16)$$

and the resonance of series circuit L_3C_1 occurs at ω_4, that is

$$\omega_4 = \frac{1}{\sqrt{L_3 C_1}} \qquad (17)$$

Combine (16) and (17), C_1 and L_3 can be derived as follow:

$$L_3 = \frac{Z_0 \omega_3}{(\omega_4^2 - \omega_3^2)} \qquad (18)$$

$$C_1 = \frac{(\omega_4^2 - \omega_3^2)}{Z_0 \omega_3 \omega_4^2} \qquad (19)$$

substitute f_1 = 3 GHz, f_3 = 10 GHz, f_4 = 13 GHz in (9), (14), (15), (18), and (19), L_1 of 2.65 nH L_2 of 1.14 nH, L_3 of 1.15 nH, C_1 of 0.13 pF, and C_2 of 0.74 pF can be obtained, and its corresponding simulated results in Fig. 13(b) exhibiting two matched frequencies (transmission poles) at 3.1 GHz and 10 GHz, and a transmission zero at 13 GHz confirms the accuracy of the formulas above.

2.3.3 Further improvement

To further improve the mid in-band S_{11}, the design methodology should be modified as follow: it appears as a high-pass circuit and meets $b_1 = x_2 = -1$ at the low matched frequency f_1 (transmission pole). Thus, the value of L_1 can be determined by (9) (i.e. $b_1 = -1$ at f_1), and the normalized reactance x_2 of L_2C_2 equals -1 as indicated in (10) (i.e. $x_2 = -1$ at f_1); besides, to achieve matched impedance at mid-band (ω_2), we should locate the resonance frequencies of the series circuit L_2C_2 and the parallel circuit $L_1C_1L_3$ at ω_2, thus Z_{in} can equal the termination resistance Z_0 (50 ohm) at ω_2:

$$L_2C_2 = \frac{1}{\omega_2^2} \tag{20}$$

$$j\omega_2(L_1 + L_3) - j\frac{1}{\omega_2 C_1} = 0 \tag{21}$$

finally, the transmission zero locates at ω_4, which is set by (14); therefore, combine (9), (10), (17), (20) and (21), L_1, L_2, L_3, C_1, C_2 can be derived as follow:

$$L_1 = \frac{Z_0}{\omega_1} \tag{22}$$

$$L_2 = \frac{Z_0\omega_1}{(\omega_2^2 - \omega_1^2)} \tag{23}$$

$$L_3 = \frac{Z_0\omega_2^2}{\omega_1(\omega_4^2 - \omega_2^2)} \tag{24}$$

$$C_1 = \frac{\omega_1}{Z_0}\left(\frac{1}{\omega_2^2} - \frac{1}{\omega_4^2}\right) \tag{25}$$

$$C_2 = \frac{(\omega_2^2 - \omega_1^2)}{Z_0\omega_1\omega_2^2} \tag{26}$$

substitute ω_1 = 3 GHz, and ω_2 = 5.4 GHz and ω_4 = 13 GHz in (22)~(26), L_1 = 2.65 nH, L_2 = 1.18 nH, L_3 = 0.55 nH, C_1 = 0.27 pF, and C_2 = 0.73 pF can be derived, and its corresponding simulated result (solid curve) shown in Fig. 14 (b), exhibits three matched frequencies: f_1 = 3.1 GHz, f_2 = 5.4 GHz, f_3 = 9.4 GHz, and one transmission zero: f_4 = 13 GHz. Thus the accuracy of (22) ~ (26) is confirmed. Specifically, at the high matched frequency f_3 (transmission pole), though the normalized susceptance b_1 of the parallel circuit $L_1C_1L_3$ is 1.42 rather than 1, and the normalized reactance x_2 is 0.94 rather 1, they still meet the matching criterion (7). As shown in Fig. 14(a), if we slightly modify one of the C_1L_3 to C_3L_4 and leave another C_1L_3 unchanged, the additional transmission zero (dashed curve) can be observed in the Fig. 14(b), where C_3 = 0.32 pF, L_4 = 0.31 nH. The proposed filter (dashed line) will be fabricated and its measurement results are shown in chapter 3.

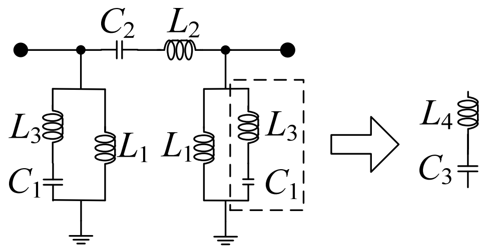

(a)

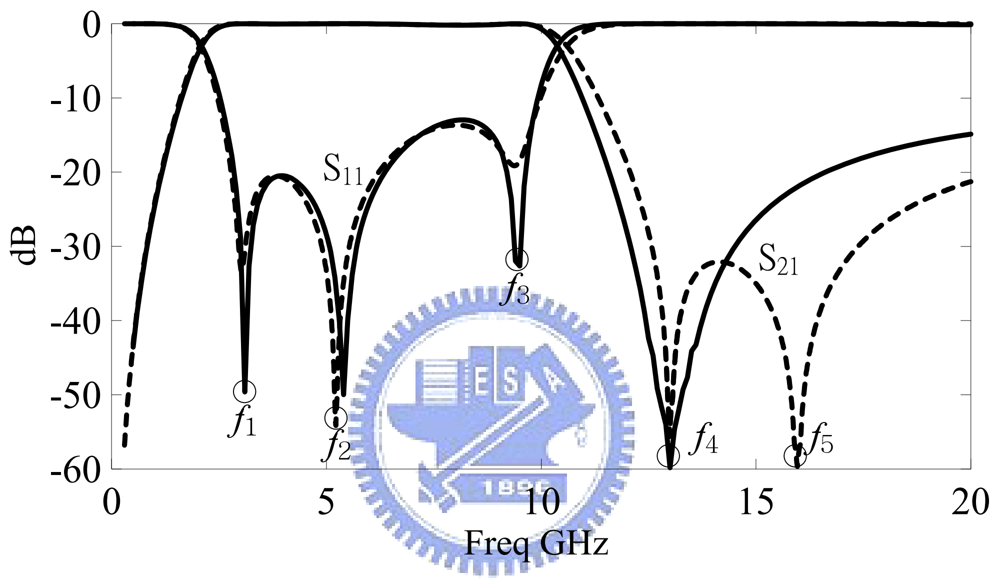

(b)

Fig. 14. (a) The proposed wideband filter. (b) The solid curve is the simulated S_{11} and S_{21} with L_1 = 2.65 nH, L_2 = 1.18 nH, L_3 = 0.55 nH, C_1 = 0.27 pF, and C_2 = 0.73 pF, where f_1, f_2, and f_3 are the three matched frequencies, and f_4 is the a transmission zero. The dashed curve is the simulated S_{11} and S_{21}, where L_4 = 0.31 nH, C_3 = 0.32 pF, and f_5 is the additional transmission zeros.

From the previous discussion, we use transmission poles to design a filter's in-band characteristic and use transmission zeros to design its stop-band characteristic. Thus, with the given transmission zeros and poles, the desired *S*-parameters of the wideband filter can be obtained. To examine the feasibility of the design methodology and the capability of the proposed wideband filter structure, a wideband filter was designed and fabricated. The measured results are shown in the next section.

Chapter 3

LAYOUT AND MEASUREMENT

3.1 Layout of the proposed filter

Proposed wideband filter mechanism has been fully analyzed in chapter 2. In this chapter, quasi-lumped elements are used to realize the proposed LC-filter. As depicted in Fig. 14(b), the inductors L_2, L_3 and L_4 are implemented by high-impedance microstrip line sections, and the shunt inductors L_1 are implemented by a short-circuited microstrip stub. The capacitors C_1 and C_3 are implemented by low-impedance microstrip line sections, and finally the series capacitor C_2 is realized by the mircostrip-to-CPW transition.

In the realization of proposed filter, the most difficult thing is to realize a series capacitor C_2 in our layout. The following are some technique to construct series capacitor. First we consider microstrip gap as our series capacitor implementation. In order to reach the desired value of capacitor C_2, the gap between two microstrip line sections will become much narrow. Due to the difficult of fabrication, microstrip gap is not suitable for our implementation. Secondly, the common used structure is interdigital capacitor which is shown in Fig. 15(a).

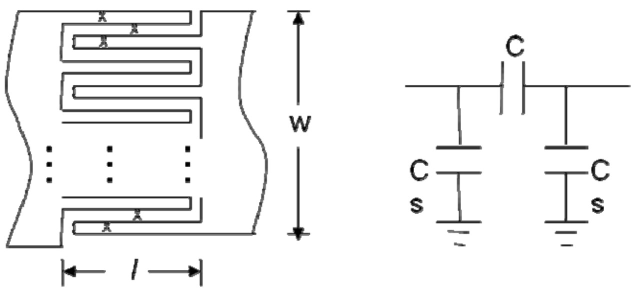

(a) (b)

Fig. 15 (a) The structure of interdigital capacitor (b) Its equivalent circuit

As shown in Fig. 15(b), the equivalent circuit of interdigital capacitor structure not only has desired series capacitor C but also accompanies two shunt parasitic capacitors C_S. From Microwave engineering, it can be derived as follow

$$C_s = 0.37\,C \qquad .(27)$$

For our proposed filter circuit in Fig. 14, the value of C is 0.75 pF and value of Cs calculated by (27) will be 0.28 pF. The value of Cs is too large for us to ignore and we find that the parasitic shunt capacitor will destroy the proposed filter performance. Thus the interdigital capacitor won't be our chose to fabricate single series capacitor. Finally, we use plate parallel capacitor to realize our circuit as shown in Fig. 16(a). It can not only produce the desired capacitor value but also eliminate the parasitic shunt capacitors. In addition, to reduce circuit size, mircostrip-to-CPW transition is used. According to the measurement result in Fig. 17, it reveals that the plate parallel capacitor is available for implementation of pure series capacitor.

The proposed wideband band-pass filter was manufactured using Rogers RO4003C (with ε_r = 3.38, tanδ = 0.0027, and thickness h = 0.508 mm). Because the proposed ultra-wideband filter in Fig. 14 only has five inductors and three capacitors, the total circuit size can be miniaturized. Fig. 16 shows the three-dimensional circuit layout, the top-/bottom-layer layout of the proposed filter, and photograph. This layout reveals how the space was efficiently utilized. Besides, for the convenience of measurement, we add two 50ohm microstrip feeding lines on the both sides of the proposed filter.

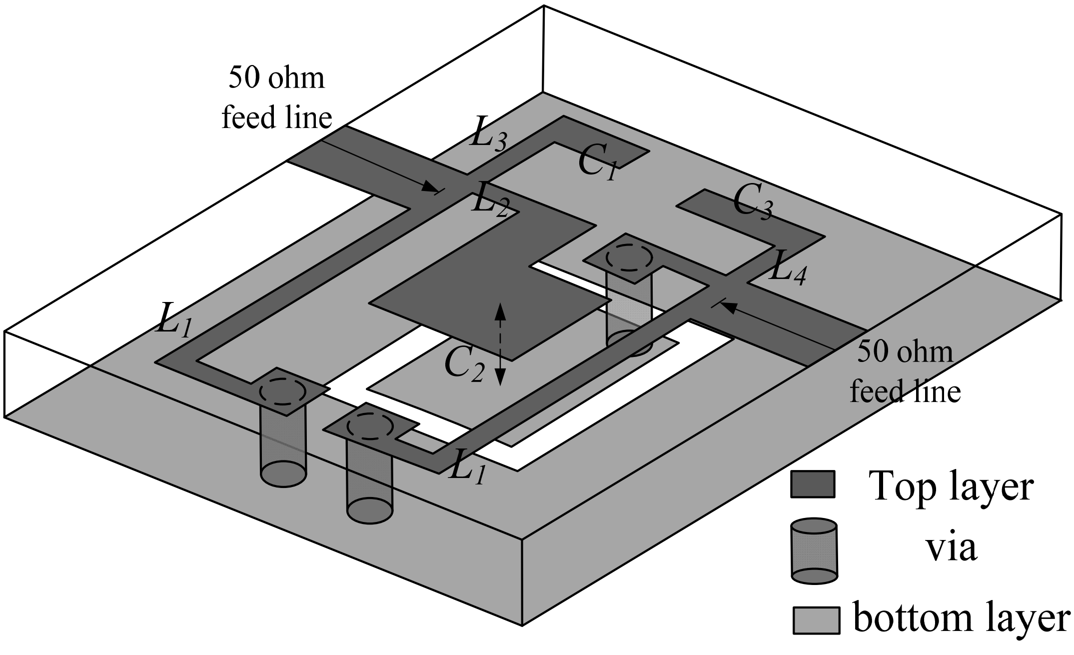
50 ohm
feed line
L_3
C_1
L_2
C_3
L_4
L_1
C_2
50 ohm
feed line
L_1
Top layer
via
bottom layer

(a)

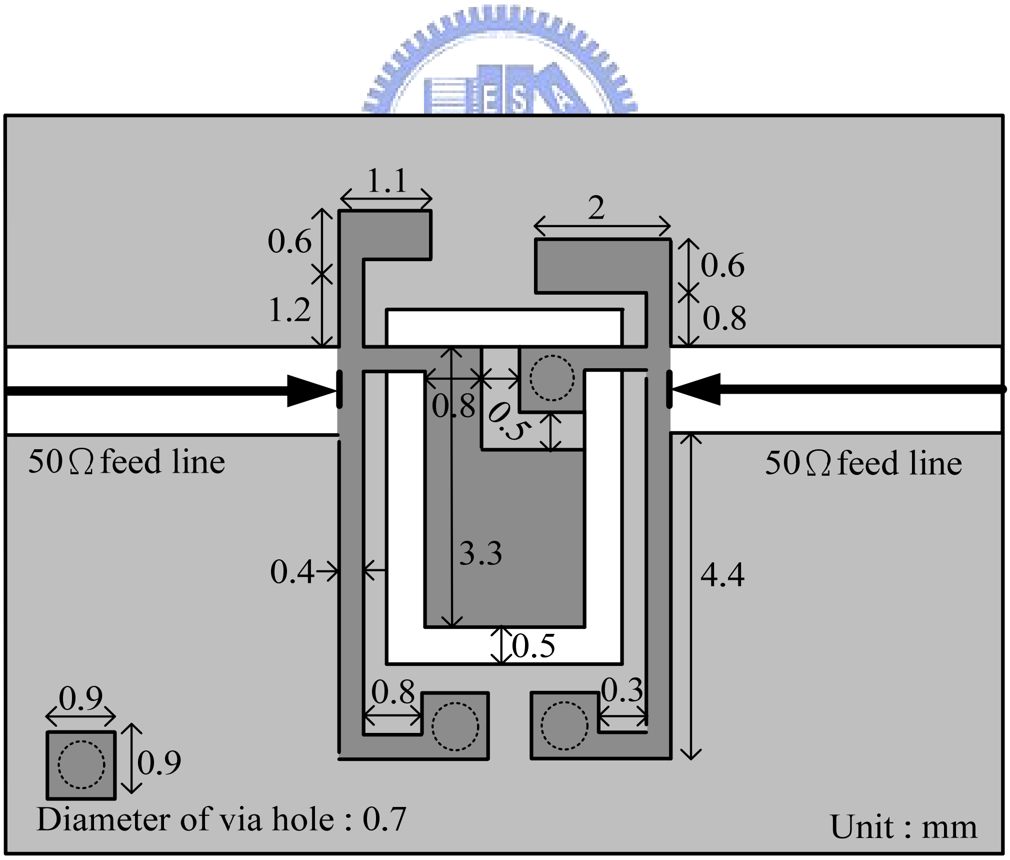
1.1
2
0.6
1.2
0.6
0.8
0.8
0.5
50Ω feed line
50Ω feed line
3.3
0.4
4.4
0.5
0.8
0.3
0.9
0.9
Diameter of via hole : 0.7
Unit : mm

(b)

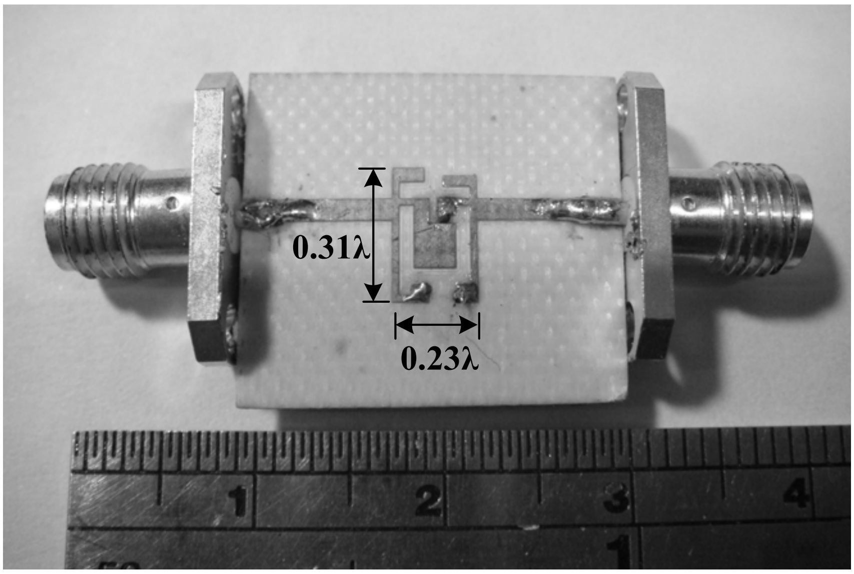

(c)

Fig. 16 (a) The three-dimensional layout. (b) The top-/bottom-layer circuit layout of the proposed filter. (c) The photograph of the filter.

The overall dimensions of these devices are 4.6 mm × 7.4 mm, which is approximately 0.23 λ × 0.31 λ, where λ is the guided wavelength of the microstrip structure at the center frequency f_0 = 7.1 GHz. The dimension confirms the very compact size of the developed device.

3.2 Measurement

The full-wave simulated result of Fig. 14 is shown in Fig. 19, which is calculated by the Ansoft HFSS simulator. Fig. 17 shows the simulated (dashed curves) and measured (solid curves) *S*-parameters of proposed wideband filter. The filter has a measured 3-dB fractional bandwidth of 128% from 2.8 GHz to 11.4 GHz. Furthermore, the return loss is greater than 11 dB within the pass-band, and the minimum insertion loss over the pass-band is 0.3 dB. It also exhibits good selectivity and stop-band rejection, which is better than 20 dB from 12.5 GHz to 24 GHz. Moreover, the implemented filter with the feeding lines exhibits flat group-delay response ranging from 0.32 ns to 0.46 ns over the whole passband as shown in Fig. 18.

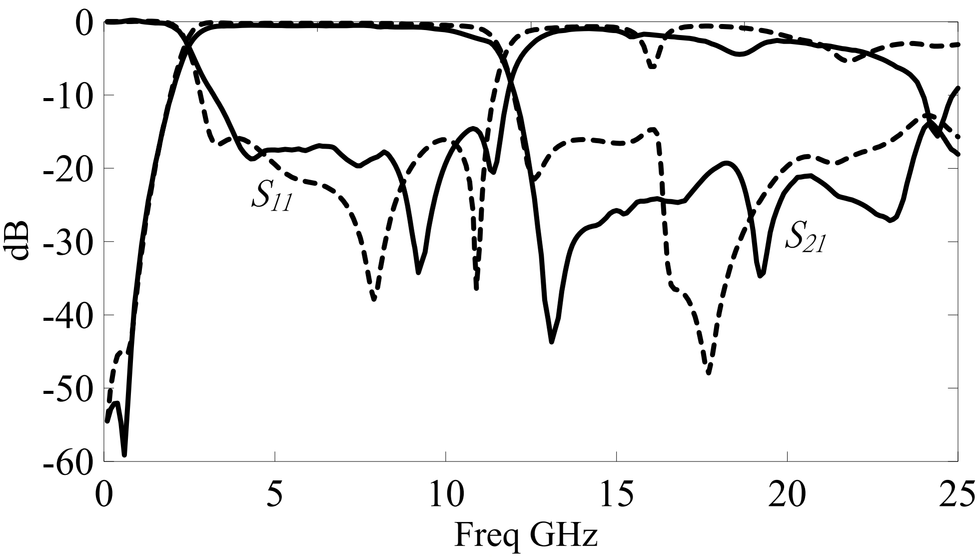

Fig. 17. Simulated (dashed curves) and measured (solid curves) insertion loss, and return loss of the fabricated filter.

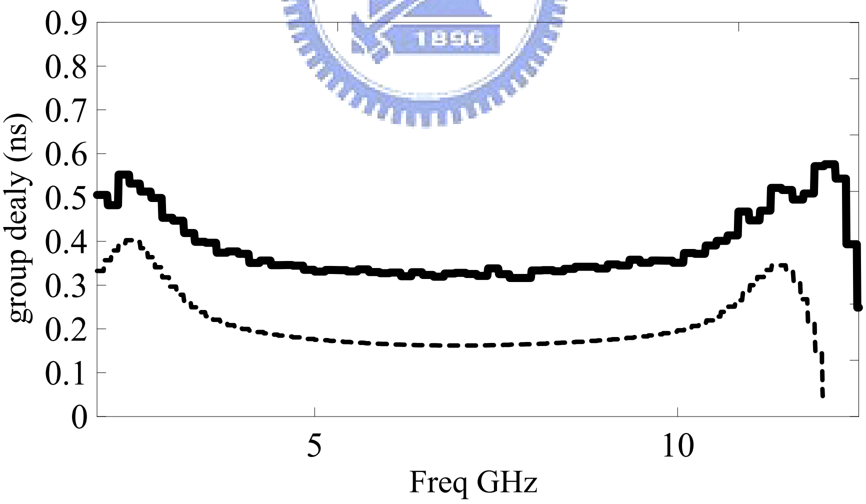

Fig. 18 Simulated (dashed curves) and measured (solid curves) group delay of the fabricated filter.

Compared with Fig. 14, the simulation results in Fig. 17 have one additional transmission zero at frequency 0.6 GHz. The reason of additional transmission zero is the coupling of adjacent inductor *L1*. Fig. 19 shows the layout of three different value of x of proposed filter and its simulation insertion loss results were shown in Fig. 20. It is clear that additional transmission zero shifts left with increasing value of x

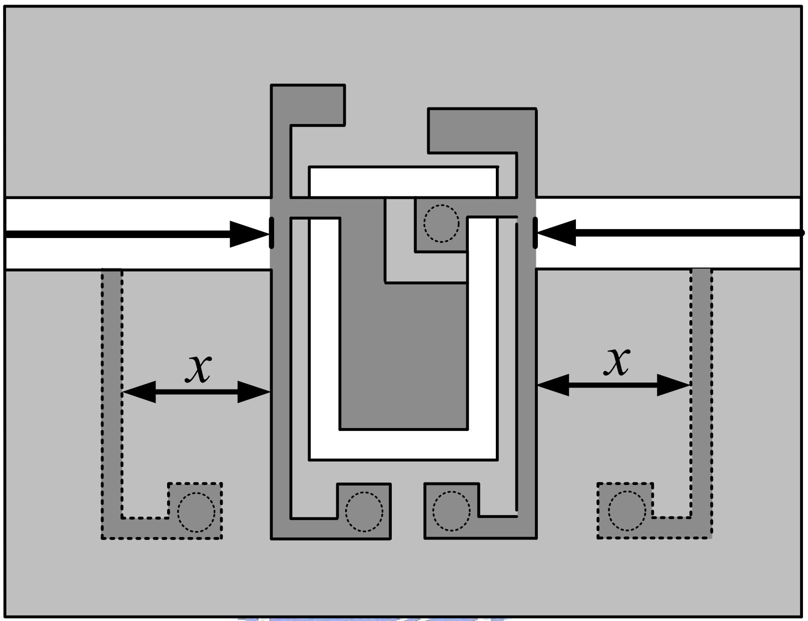

Fig. 19. The top-/bottom-layer circuit layout of x=2 (circled curve), x=1 mm (dashed curves), and x=0 (solid curves) of the fabricated filter.

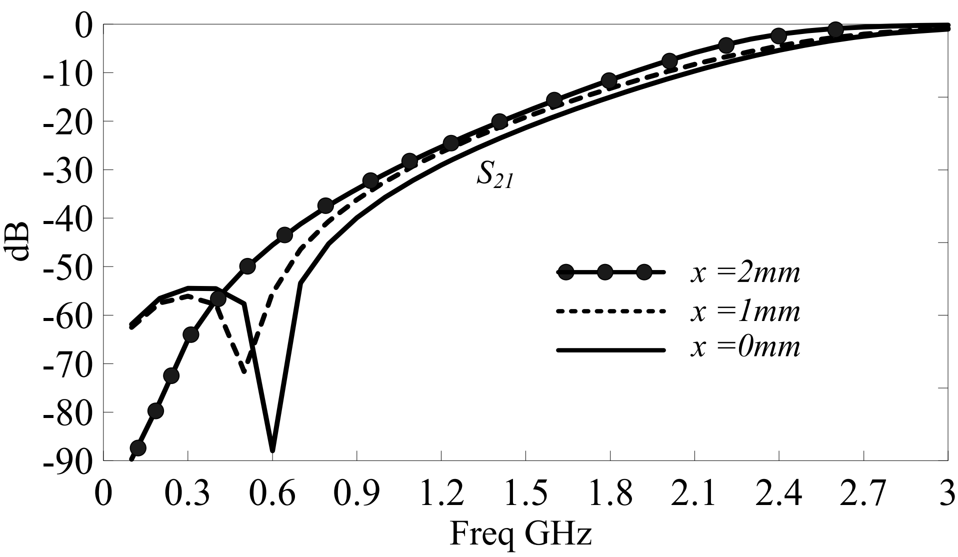

Fig. 20. The simulated insertion loss with x=2 (circled curve), x=1 mm (dashed curves) and x=0 (solid curves) of the fabricated filter.

When compared with other publications in Table 3, initially we find that 3-dB bandwidth of UWB filters which were proposed in [8] ~ [11] vary from 108% to 139%., and 128% of the UWB filter we proposed. Secondly, concern about the stopband rejection, it is clear that the filters shown in Table [3] all have good out-of-band rejection of least 20 dB. Thus, it doesn't make much difference in the performance of 3-dB bandwidth and stopband rejection. But the most important thing is that the UWB filter we proposed has the most compact circuit size compared with others. Therefore, the proposed compact ultra-wideband filter is promising for communication application.

Ref.	**3-dB bandwidth**	**stopband rejection (20dB)**	**Circuit size**
In [8]	108% (3 GHz~10GHz)	12.4GHz~20GHz	$0.16\lambda \times 0.64\lambda$
In [9]	110% 3GHz~10.4GHz	12.6GHz~26.9GHz	$0.45\lambda \times 1.76\lambda$
In [10]	130% 1.2GHz~5.6GHz	6.4GHz~20GHz	$0.28\lambda \times 0.59\lambda$
In [11]	108% 3GHz~10.1GHz	10.7GHz~20GHz	$0.4\lambda \times 0.7\lambda$
In [12]	139% 1.8GHz~10.1GHz	10.4GHz~18GHz	$0.36\lambda \times 0.87\lambda$
This paper	**128% (2.8GHz~11.4GHz)**	**12.5GHz~24GHz**	$\mathbf{0.23\lambda \times 0.31\lambda}$

Table. 3 Comparision with other publication in 3-dB bandwidth, stopband rejection, and circuit size

Chapter 4
CONCLUSION

4.1 Conclusion

In this paper, a simple design methodology for a compact ultra-wideband filter with wide-stopband has been thoroughly analyzed. By treating filter as a π-network circuit and solve the matching mechanism by using Smith chart. With the given specification, the desired value of each LC component can be calculated by equation (22) ~ (26).

On the other hand, to examine the feasibility of the design methodology and the capability of the proposed wideband filter structure, a wideband filter was designed and manufactured. By using quasi-lumped element and mircostrip-to-CPW transition, the layout of the proposed filter is designed. The measured results show that the filter prototype has 3-dB fractional bandwidth of 128% from 2.8 GHz to 11.4 GHz. Furthermore, the return loss is greater than 11 dB within the pass-band, minimum insertion loss of 0.3 dB over the pass-band, superior 20 dB stop-band rejection to above 24 GHz, flat group delay of 0.4 ns within 0.15 ns variation over the pass-band, and very compact circuit size of 0.23 λ × 0.31 λ, where λ is the guided wavelength of the microstrip structure at the center frequency f_0 = 7.1 GHz.

APPENDIX

As shown in Fig. 2(a) shows the mechanism of the π-network, and its S_{11} and S_{21} are solved by *ABCD* matrix as follow [12]:

$$S_{11} = \frac{A + \frac{B}{Z_0} - CZ_0 - D}{A + \frac{B}{Z_0} + CZ_0 + D} \tag{28}$$

$$S_{21} = \frac{2}{A + \frac{B}{Z_0} + CZ_0 + D} \tag{29}$$

where Z_0 is the ubiquitous microwave 50-ohm and

$$\begin{aligned} A &= D = 1 - x_2 b_1 \\ B &= j x_2 Z_0 \\ C &= j(2b_1/Z_0 - b_1^2 x_2/Z_0) \end{aligned} \tag{30}$$

where b_1 is the normalized susceptance of the capacitor, x_2 is the normalized reactance of the inductor. Let $|S_{11}|^2 = 0$ or $|S_{21}|^2 = 1$, we can get

$$x_2 = \frac{2b_1}{1 + b_1^2} \tag{31}$$

The matching criterion (31) is identical to (7)

REFERENCE

[1] H. Ishida, and K. Araki, “Design and analysis of UWB filter with ring filter,” in *IEEE MTT-S Int. Microw. Symp. Dig.*, Jun. 2004, pp. 1307–1310.

[2] L. Zhu, H. Bu, and K. Wu, “Aperture compensation technique for innovative design of ultra-broadband microstrip bandpass filter,” in *IEEE MTT-S Int. Microw. Symp. Dig.*, Jun. 1999, pp. 315–318.

[3] W. Menzel, L. Zhu, K.Wu, and F. Bogelsack, “On the design of novel compact broadband planar filters,” *IEEE Trans. Microwave Theory Tech.*, vol. 51, no. 2, pp. 364–369, Feb. 2003.

[4] J. T. Kuo and E. Shih, “Wideband bandpass filter design with three-line microstrip structures,” in *IEEE MTT-S Int. Microw. Symp. Dig.*, 2001, pp. 1593–1596.

[5] L. Zhu, S. Sun, and W. Menzel, “Ultra-wideband (UWB) bandpass filters using multiple-mode resonator,” *IEEE Microw Wireless Compon. Lett.*, vol. 15, no. 11, pp. 796–798, Nov. 2005.

[6] H. Wang, L. Zhu, and W. Menzel, “Ultra-wideband bandpass filter with hybrid microstrip/CPW structure,” *IEEE Microw. Wireless Compon. Lett.*, vol. 15, no. 12, pp. 844–846, Mar. 2005.

[7] J. Gao, L. Zhu, W. Menzel, and F. Bögelsack, “Short-circuited CPW multiple-mode resonator for ultra-wideband (UWB) bandpass filter,” *IEEE Microw. Wireless Compon. Lett.*, vol. 16, no. 3, pp. 104–106, Mar. 2006.

[8] C. L. Hsu, F. C. Hsu, and J. T. Kuo, “Microstrip bandpass filter for ultra-wideband (UWB) wireless communications,” in *IEEE MTT-S Int. Microw. Symp. Dig.*, 2005, pp. 679–682.

[9] C. W. Tang and M. G. Chen, “A microstrip ultra-wideband bandpass filter with cascaded broadband bandpass and bandstop filters,” *IEEE Trans. Microw. Theory Tech.*, vol. 55, no. 11, pp. 2412–2418, Nov. 2007.

[10] H. N. Shaman and J.-S. Hong, “Compact wideband bandpass filter with high performance and harmonic suppression,” in *37th Eur. Microw. Conf.*, 2007, pp. 528–531.

[11] J. Garcia-Garcia, J. Bonache, and F. Martin, “Application of electro- magnetic bandgaps to the design of ultra-wide bandpass filters with good out-of-band performance,” *IEEE Trans. Microw. Theory Tech.*, vol. 54, no. 12, pp. 4136–4140, Dec. 2006.

[12] Z. C. Hsu, and J. S. Hong, “Ultra-wideband bandpass filter using multilayer liquid-crystal-polymer technology ,” *IEEE Trans. Microwave Theory Tech.*, vol. 56, no. 9, pp. 2095–2100, Sep. 2008.

[13] S. Cripps, “Microwave bytes: naïve filter design,” *IEEE Microwave. Magazine,* vol.7, issu. 4, pp. 30-36, Aug. 2006.

[14] D. Pozar*, Microwave Engineering*, 3rd ed. New York: Wiley, 2005.